Electronic Supplementary Material (ESI) for RSC Advances.

Aggregation of Catalytically Active Ru Nanoparticles to Inactive Bulk, Monitored In Situ During Allylic Isomerization Reaction. Influence of Solvent, Surfactant and Stirring.

*M. Hitrik and Y. Sasson**

Supporting Information

Section SI 1. *Experimental.*

SI 1.1 The catalyst (the complex) synthesis.

$Ru_3O(OCOCH_3)_6(H_2O)_3][OCOCH_3]$ was prepared from commercially available ruthenium trichloride trihydrate, according to a procedure based on the one given by Wilkinson and co-worker.[25, 26] 4 g of $RuC1_3$, xH_20, together with 7 g of $NaOCOCH_3$, $3H_2O$, were dissolved in a mixture of 75 ml glacial acetic acid and 75 ml of ethanol. The solution was refluxed under nitrogen for approximately 2 h, and the initial reddish-brown color of the solution changed to dark green. The solution was cooled to -30^{o}C and decanted to separate precipitated sodium chloride and sodium acetate. The decanted solution was then filtered and the filtrate was taken to dryness. The solid thus obtained was the crude oxo-triruthenium(III) acetate complex. The resulting crude acetate complex was dissolved in a minimum amount of ethanol and cooled overnight to -30^{o}C. Sodium acetate and sodium chloride were precipitated and separated by filtration. The filtrate was taken to dryness and the solid was washed with benzene to remove excess acetic acid. Several extractions with ethanol were performed until no more precipitate was apparent on filtration. This final filtrate was taken to dryness, and after a final benzene wash the product was dried overnight in vacuum over sodium hydroxide pellets at 60^{o}C. The yield was 3.2 g (80% on the basis of Ru content of $RuCl_3$, xH_2O).

SI 1.2. Reaction conditions:

b)- with stirring: A number of experiments were performed with the same reaction conditions as in Exp. 1 but with addition of fast stirring - 250 rpm: a magnetic stirrer was placed inside the reaction flask.; the concentrations of reactant 1 and the complex were from the same ranges as signed in the Experiment 1.

c)- with Aliquat 336 as a surfactant: Before addition of substrate, a small volume of aliquat 336, at the excess concentration from 0.043 M to 0.18 M, was injected to the reaction flask with a solvent and complex. After that, the Background measurement was taken and 1-octen-3-ol was added. The [reactant $1]_0$ and [complex] were the same like in Exp. b.

d)- with aliquat 336 and stirring: procedure - the same as Exp. c ([reactant $1]_0$ range and $[\text{complex}]_0$) and the magnetic stirrer was injected into the flask and was activated during reaction propagation (250 rpm). The excess aliquat concentrations were from the range from 0.043 M to 0.18 M.

SI 1.3 Methods

Method of monitoring of reaction profiles. The absorbance values collected from on-line IR profile-spectra were converted to the concentration of the product of the reaction 1 using calibration plot. The calibration blot of absorbance vs. concentration was built separately for each solvent at the relevant linear range of concentrations.

Method of study of reaction mixture. GC used for mixture analysis was from FOCUS type equipped with dimethylpolysiloxane 95% and diphenyl 5% capillary column (30 m/0.25 mm) with FID detector. GSMS analysis was performed with HP-

G1800B with dense column comprised of dimethylpolysiloxane 95% and diphenyl 5%, FID. Injector temperature was 280 °C, detector temperature – 280 °C.

Methods of NPs *characterizations.* TEM (High Resolution Transmission Electron Microscopy) *(47)* - A drop of the solution was placed onto a carbon-coated copper grid and allowed to evaporate. TEM experiments were performed using a TECNAI F20 G^2, from FEI, USA*(47-a)*, point resolution 0.24 nm, line resolution 0.1 nm, limit of information 0.15 nm.

SEAD (Selected Area Diffraction) pattern- using diffraction process provides a basis for studying the structure of crystals and of identifying materials (TEM Tecnai F20 G^2).

DLS (Dynamic Light Scattering) - Nano-S (Nano-Sizer, λ=633 nm; Malvern Instruments, UK) instrument was used. The measurements were carried out at a scattering angle of 173° at 25° C. Data were collected in 3 repeated measurements (10 scans for each repeat). The average size was reported by the number distribution (statistics) for each measurement.

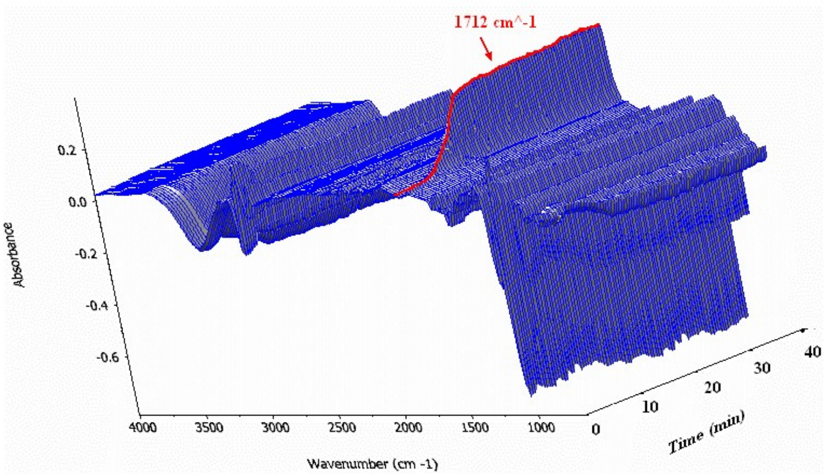

Figure SI 1. The 3D profile obtained with ATR-FTIR monitoring of reaction 1 propagation. The most noticeable change of the absorbance was obtained with the wavenumber of 1712 cm-1, which corresponds to the C=O bond formation, found at the reaction 1 product – 3-octanone.

Section SI 2. *Analysis of reaction 1 products and byproducts.*

The composition of the final reaction mixture was analyzed to check the formation of possible byproducts. Reaction of allylic alcohol isomerization of 1-octene-3-ol may generate three products - 3-octanone, 1-octene-3-one and 3-octanol. The latter two are considered as side products.

Distinguishing between the starting material and these three products using ATR-FTIR might be a challenging task since they have the same functional groups in IR spectrum (-OH, -C=C-, -C=O, -C-C-, -C-H). In addition, the concentrations of the side products in this case are very low. Absorbance peaks are concentration-dependent; thus IR spectroscopy is not useful here. Therefore, to assay the presence of byproducts and to determine their concentrations, we have used GC-MS. The samples of the reaction mixtures in all conditions, solvents, and initial compositions were analyzed in GC-MS at the end of the process. The resulting spectra in all the examples looked the same way – one high and wide peak (99.38%) appeared with a small, narrow peak close to it (0.62%). The integration and calibration technique was performed using GC instrument for estimation of the real peaks molar ratio. The large peak was scanned and the resultant compositions were from two types. In the cases with full substrate conversions, mass fragments of main product only – 3-octanone – were observed (Figure SI 2).

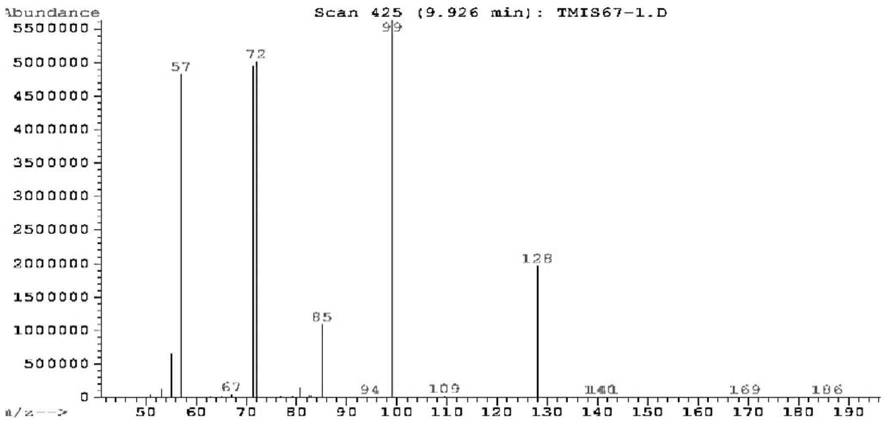

Figure SI 2. The MS spectra that corresponds to the main product of reaction 3-octanone.

Scanning the high peak in the cases with partial conversions gave two spectra with different mass fragments: one of main product and another of substrate – 1-octene-3-ol (Figure SI 3). These spectra were compared to literature (NIST, National Institute of standards and technology, http://webbook.nist.gov).

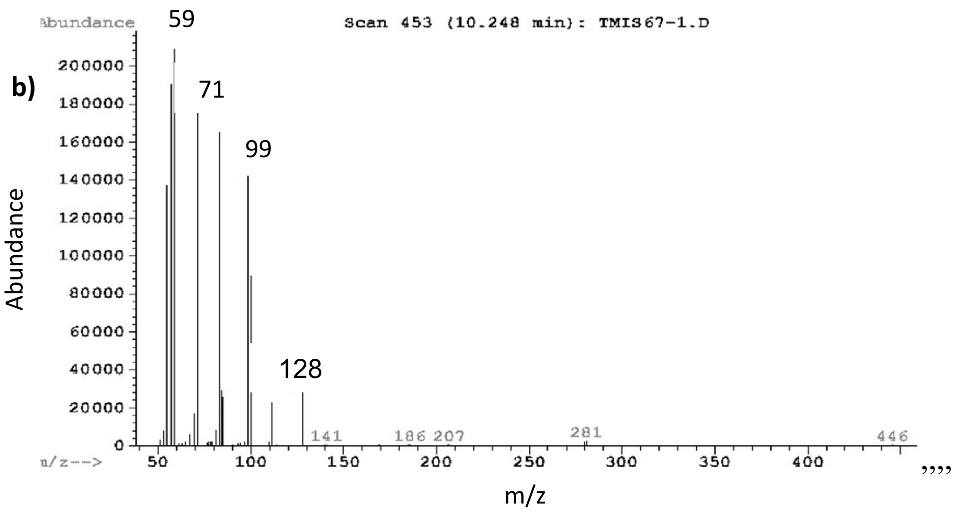

Figure SI 3. The MS spectra that corresponds to the reactant of reaction 1-octene-3-ol.

These two species have almost the same retention time, because of their similarity in physical properties. Thus, at the elution from the column two corresponding peaks accreted, even in the slow rate of temperature progression (starting from 25 ^{o}C, 0.5 $^{o}C/min$).

The small peak was then scanned to find out its composition. It was realized that in all cases only one type of mass spectrum performed in this peak and it suites to the side product of reaction 1 – 3-octanol (Figure SI 4).

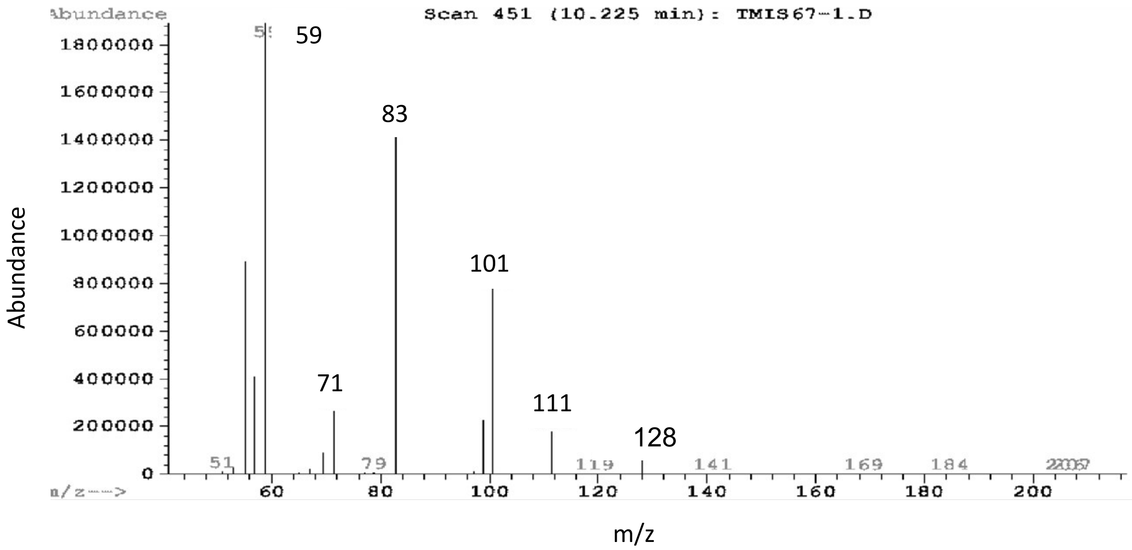

Figure SI 4. The MS spectra that corresponds to the byproduct of reaction 3-octanol.

An integration of the corresponding peaks showed that the relative ratio of the side product is < 1 mole%, independent on conversion. Thus, 3-octanol was formed only in trace amounts and has almost no influence on the overall reaction behavior, and may be neglected. No other peaks appear in GC/MS spectra, hence 1-octene-3-one was not formed during the reaction, or its concentration is negligible.

The summary of experimental results from IR, GC and GC/MS measurements:

The absence of intermediates and negligible amounts of the side products permit the use of the product concentration profile with time alone as the reaction profile for kinetic analysis propose and rate constants calculations (it is exactly "reverse" to substrate consumption profile).

The existence of induction period for all reaction species indicates that complex 1 is catalytically inactive during this initial reaction stage. This is one of the evidences for catalytic nanoclusters in-situ formation.

The reaction profile is of sigmoidal shape. This signs out that an autocatalysis is involved in the reaction mechanism. This is also typical for catalysis by in situ formed NPs. (*Besson, C.; Finney, E. E.; Finke R. G. J. Am. Chem. Soc.* ***2005****, 127, 8179-8184*).

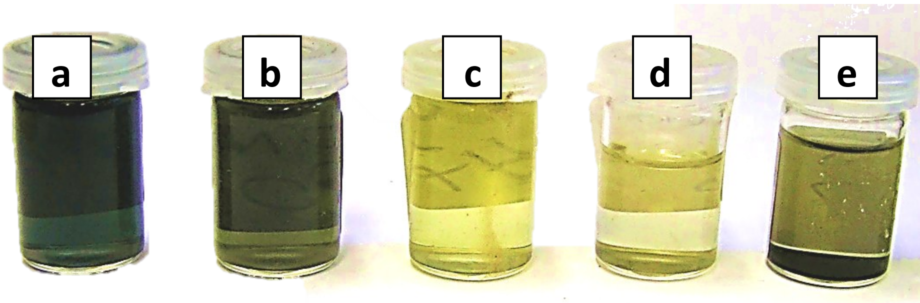

Figure SI 5. Visual color change of the reaction solution

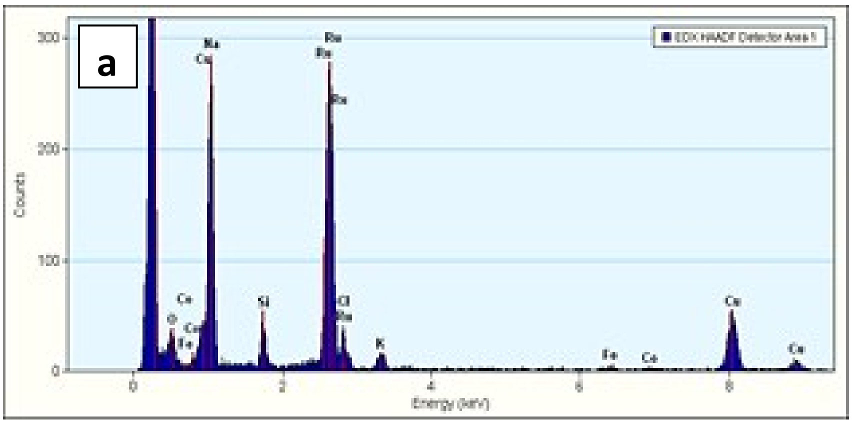

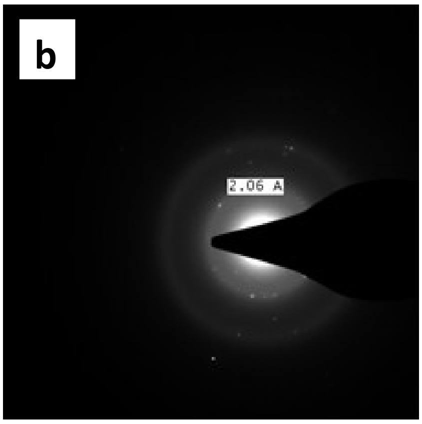

Figure SI 6. EDAX and SAD analysis: Reaction 1 mixture at the end of the reaction, in iso-propanol as a solvent. T=80°C, TON=$2x10^5$, [catalyst 1]=$1.9x10^{-5}$(M), Conversion = 0.45: a – EDAX results of the dried drop of the solution on the copper grid; b - SAD results of the agglomerated particle (in iso-propanol, TON=$2*10^5$, Conversion = 0.45). The strongest d =2.06 (A) was measured, where d is the crystal lattice spacing between atomic planes. Reaction mixture at the end of the reaction, in iso-propanol as a solvent.

Number of exp.	Solvent	[1-octene-3-ol] (M)	[catalyst (1)] (M)	Induction time (min)	Conversion.
1	ethanol	3.2	$0.74*10^{-4}$	9	1
2	ethanol	3.2	$0.8*10^{-3}$	17	1
3	ethanol	3.2	$1.72*10^{-4}$	25	1
4	n-pent.	0.91	$1.8*10^{-4}$	10	0.85
5	n-pent.	0.91	$0.12*10^{-3}$	25	0.82
6	n-pent.	0.91	0.001	30	1
7	iso-prop.	2.6	$1.7*10^{-5}$	16	0.92
8	iso-prop.	2.6	$3*10^{-4}$	19	1
9	iso-prop.	2.6	$1.3*10^{-4}$	29	1

Table SI 1. Summary of induction period length at different reaction conditions. No clear correlation can be seen

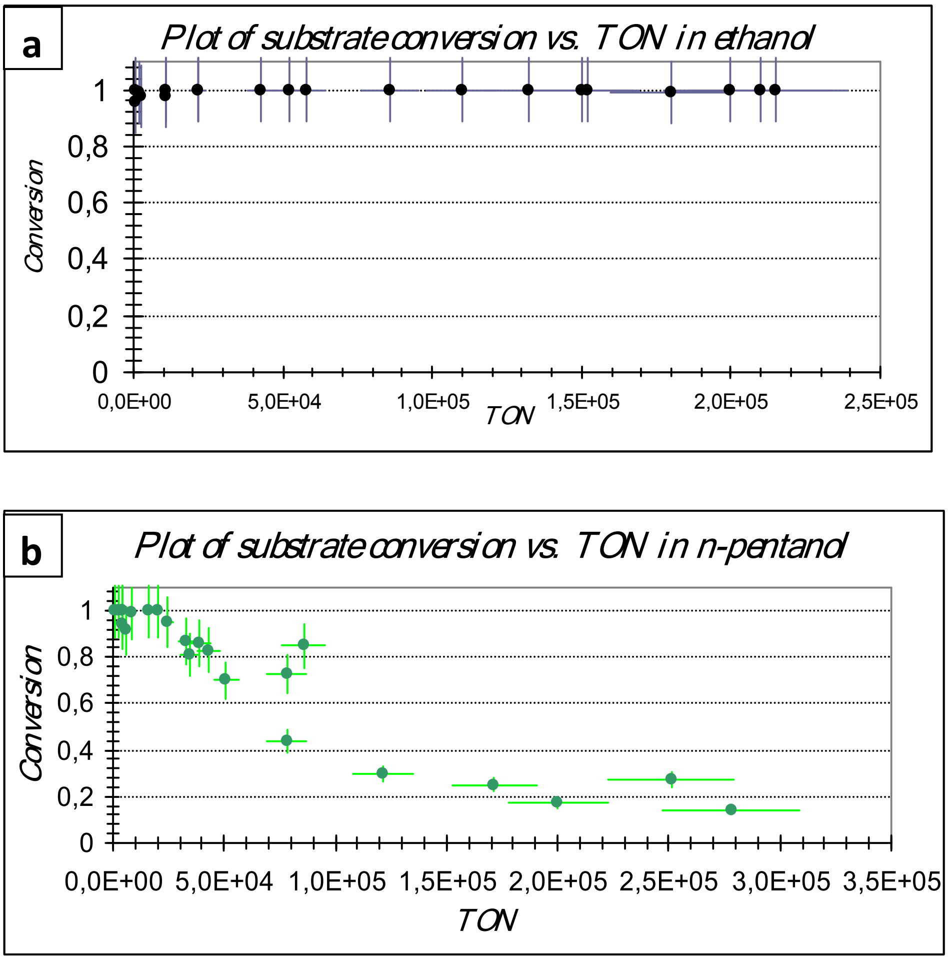

Figure SI 7. Plots of Conversion vs. TON of reaction 1 obtained with: a - iso-propanol and b - n-pentanol solvents.

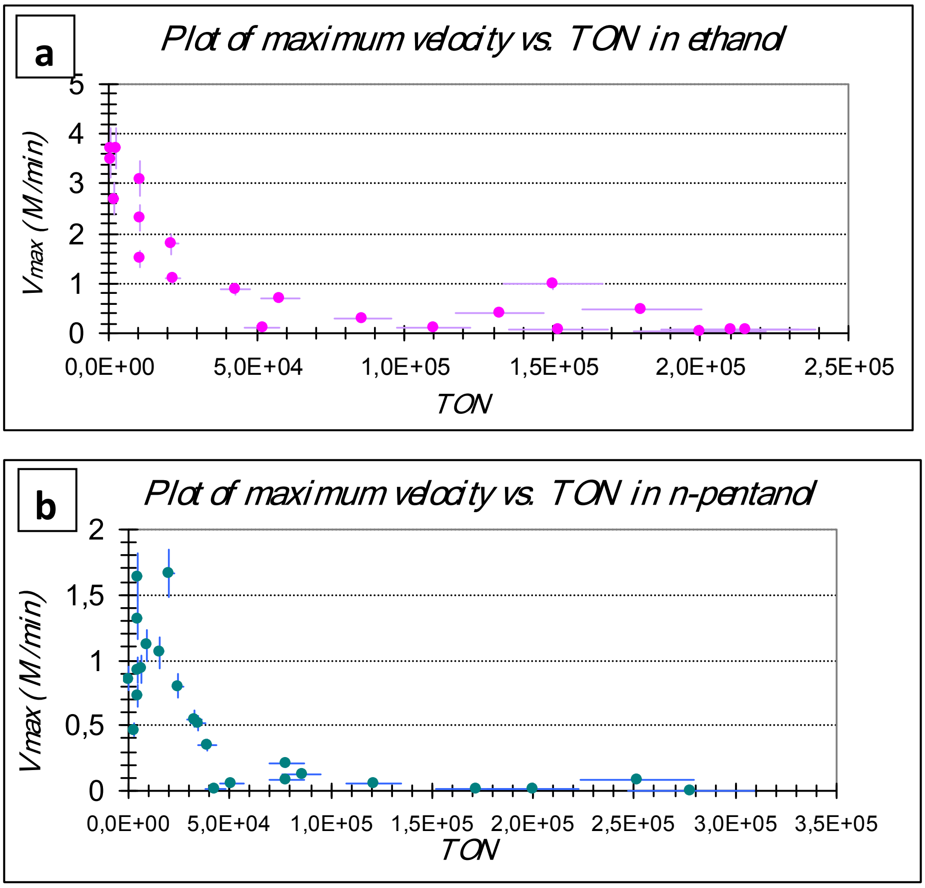

Figure SI 8. Maximal velocities obtained at different TON of reaction 1 in: a – ethanol, b – n-pentanol, as a solvent.

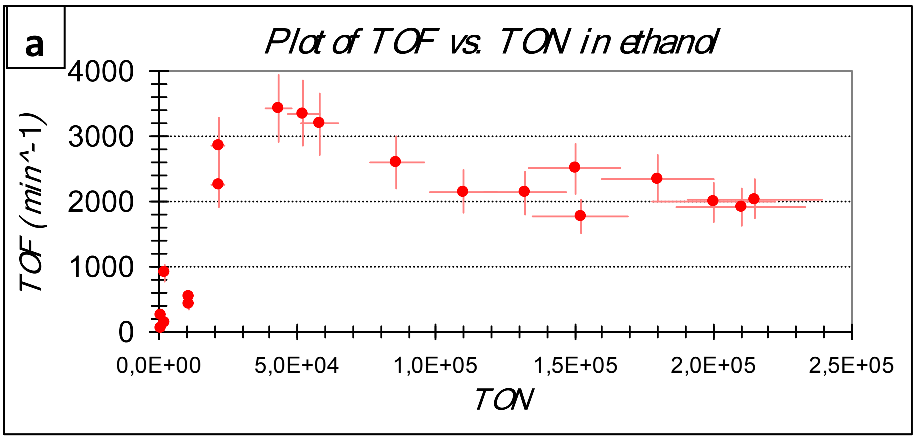

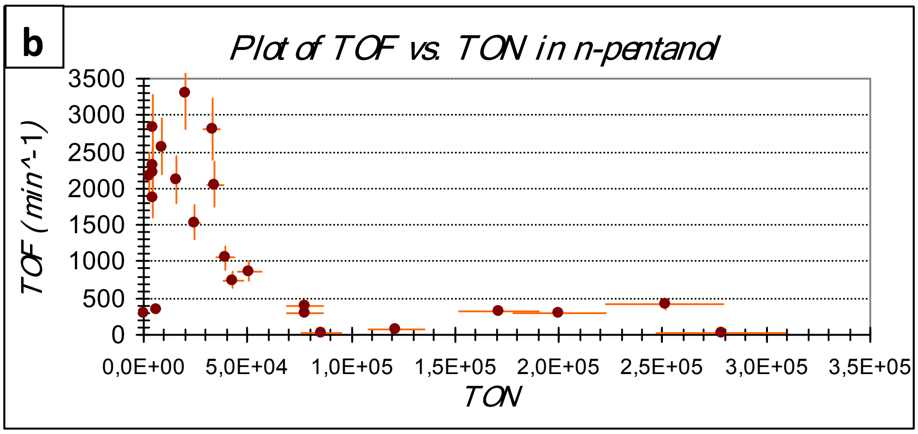

Figure SI 9. The plots of TOF vs. TON of reaction 1 in: a – ethanol, and b – n-pentanol, as a solvents.

Section SI 10. Optimization of the kinetic mechanism to find the best fit to the experimental results.

In this work, we use the model of pseudo-elementary step mechanism purposed by Finke-Watzky and developed by Noyes. In this mechanism we summarize all the catalytic steps to Reactant+catalyst → Product+catalyst, as the needed concentration of catalyst is in the equal stochiometric ratio, as the reactant, to give one molecule of the product. In addition, in the first step A represents *n* complexes of precatalyst and in the second stage A represents a single mol of the precatalyst. However, using this model, the extrapolation of the kinetic rate constants becomes as a relatively easy task, and this was proved as a sufficient tool of solution of multi-step complex kinetic mechanisms. Using this model it is possible to compare between different reactions and to learn their kinetic parameters.

In all the putative mechanisms, there are two types of NPs present - B and C that differ in size. Therefore, both of them should be checked on their potential catalytic activity in reaction 1 (A cannot be the true reaction catalyst due to well-defined induction time, and D was defined to be inactive). For this aim two variations of _Mechanism to test_ - _(1)_ and _(2)_ are introduced and analyzed as follows:

_(1)_: $\mathbf{R} + \mathbf{B} \xrightarrow{k_7} \mathbf{B} + \mathbf{P}$, where S is the substrate (1-octene-3-ol) and P is the product (3-octanone), B is the true reaction catalyst.

_(2)_: $\mathbf{R} + \mathbf{C} \xrightarrow{k_8} \mathbf{C} + \mathbf{P}$, where C is the true reaction catalyst.

The probability of double-cycle catalysis by B and C NPs was also tested – _(3)_. It is known that catalytic activity of NPs is strongly dependent of their size. Previous experience showed the existence of an optimal size and geometry of the NPs that gives the best activity and efficiency for specific chemical reactions *(T. Matsumoto, M. Ueno, J. Kobayashi, H. Miyamura, Y. Mori, S. Kobayashi, Adv Synth Catal.* ***2007****, 349, 531).* Nevertheless, NPs of the slightly smaller or bigger sizes are catalytically active either, but weaker and slower than the most active type. If the NPs assemble in situ, like in our case, there is a range of the sizes (nm) presents in the reaction mixture. Here, probably, more than one-size of particles is catalytically active. Thus, in the studied case the situation of two different types of reaction catalysts- B and C - is possible. One of them probably is more active than the other. The term of 'true reaction catalyst' is remained to emphasize the most active form.

Mechanism A – the classical mechanism of NPs self-assembly, without reflection on the complex structure of Ru precatalyst, see Table SI 2.

In *Mechanism B* takes into account the tripe-metallic center of the catalyst 1, in the terms of the second step of surface growth of the B particle – here the growth step occurs via addition of two Ru^0 atoms. And then the mechanism propagates as mechanism A

The next proposed mechanism - *Mechanism C* – is based on the idea that at the beginning only one Ru metal salt center is reduced until the "saturation level." Only then, two others that remained in complex 2 are reduced. Consequently, if the first center (A) is reduced to form NPs (B), the following autocatalytic step (A+B → 2B) of reducing this first metal center (A) should begin, before the other two metals in complex 1 react. That is to say, the *Mechanism C* is triple autocatalytic, and may be entered as shown below.

Complex 2:

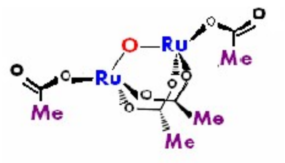

Mechanism C

1) reduction of the first Ru^{+3} to Ru^0 nanocluster:

$$A \xrightarrow{k_1} \mathrm{B}$$

2) first autocatalysis: autocatalytic surface growth (by one) of nanoclusters that already have formed (B) by the same first center of Ru^{+3} (A). Other two metallic centers – complex 2- are still untouched.

$$\mathrm{A} + \mathrm{B} \xrightarrow{k_2} 2\mathrm{B}$$

3) second autocatalytic step: autocatalytic reduction of remained two metal centers (=2*X) in complex 2 by formed nanoclusters (B) to give NP surface growth (by two). The special symbol-X is needed because now A and X are independent species. Then

$$2\mathrm{X} + \mathrm{B} \xrightarrow{k_3} 3\mathrm{B}$$

concentration of A decreases, concentration of X stays constant or declines by its own rate. ($[X]_0=[A]_0$)

4) $2B \xrightarrow{k_4} C$

5) $B + C \xrightarrow{k_5} 1.5C$

6) agglomeration to bulk metal – for experimental curves in pentanol and iso-propanol solvents.

$$2C \xrightarrow{k_6} D$$

Another possible mechanism- *Mechanism- D* that was based on the fact that the saturation level presented in the reduction of Oxo-triruthenium acetate is not compete (Figure 33). Hence, the species A and X probably are not independent, like in *Mechanism C* (where X is entered as independent variable with its own $[X]_0$, as if it was injected in to reaction flask), and should be entered in the following, dependent way.

Mechanism- D

1) nucleation step: first metal center Ru(3+) (= A) is reduced to give Ru(0) NPs and complex 2(= X)

$$A \xrightarrow{k_1} B + X$$

2) first autocatalytic step: first metal center (A) reduced by NPs (B) catalysis to give surface growth of nanocluster (B) and complex 2 –X.

$$A + B \xrightarrow{k_2} 2B + X$$

3) second autocatalytic step: metal centers in complex are reduced to give NPs growth

$$X + B \xrightarrow{k_3} 3B$$

4) $2B \xrightarrow{k_4} C$

$$B + C \xrightarrow{k_5} 1.5C$$

5)

6) $2C \xrightarrow{k_6} D$ - only for n-pentanol and iso-propanol solvents

In Table SI 2, the list of all potential mechanisms is presented.

Table SI 2. Iterated mechanisms.

Mechanism A			*Mechanism B*		
$A \rightarrow B$, k_1 $A+B \rightarrow 2B$, k_2 $2B \rightarrow C$, k_3 $B+C \rightarrow 1.5C$, k_4 $C+C \rightarrow D$, k_5 (for n-pent., iso-prop.)			$A \rightarrow B$, k_1 $2A+B \rightarrow 3B$, k_2 $2B \rightarrow C$, k_3 $B+C \rightarrow 1.5C$, k_4 $C+C \rightarrow D$, k_5 (for n-pent., iso-prop.)		
A(1)	*A(2)*	*A(3)*	*B(1)*	*B(2)*	*B(3)*
$R+B \rightarrow P+B$ k_7	$R+C \rightarrow P+C$ k_8	$R+B \rightarrow P+B$ k_7 $R+C \rightarrow P+C$, k_8	$R+B \rightarrow P+B$ k_7	$R+C \rightarrow P+C$ k_8	$R+B \rightarrow P+B$ k_7 $R+C \rightarrow P+C$ k_8

Mechanism C			*Mechanism D*		
$A \rightarrow B$, k_1 $A+B \rightarrow 2B$, k_2 $2X+B \rightarrow 3B$, k_3 $2B \rightarrow C$, k_4 $B+C \rightarrow 1.5C$, k_5 $C+C \rightarrow D$, k_6 (for n-pent., iso-prop.)			$A \rightarrow B+X$, k_1 $A+B \rightarrow 2B+X$, k_2 $X+B \rightarrow 3B$, k_3 $2B \rightarrow C$, k_4 $B+C \rightarrow 1.5C$, k_5 $C+C \rightarrow D$, k_6 (for n-pent., iso-prop.)		
D(1)	*D(2)*	*D(3)*	*D(1)*	*D(2)*	*D(3)*
$R+B \rightarrow P+B$ k_7	$R+C \rightarrow P+C$ k_8	$R+B \rightarrow P+B$ k_7 $R+C \rightarrow P+C$ k_8	$R+B \rightarrow P+B$ k_7	$R+C \rightarrow P+C$$k_8$	$R+B \rightarrow P+B$ k_7 $R+C \rightarrow P+C$ k_8

For testing and optimization of these mechanisms, the Macintosh program MacKinetics was used. This program can fit models of mechanism to the experimental data – in our case this is the concentration profile of 3-octanone. The best-fitted values of kinetic rate constants appear in the output window with the corresponding residual number. The decision about the best mechanism is done by the combination of the smallest residual number and visual appropriateness.

After checking all of the possible mechanisms, the most appropriate was obtained. This is *Mechanism D(3)* with C as a true reaction catalyst.

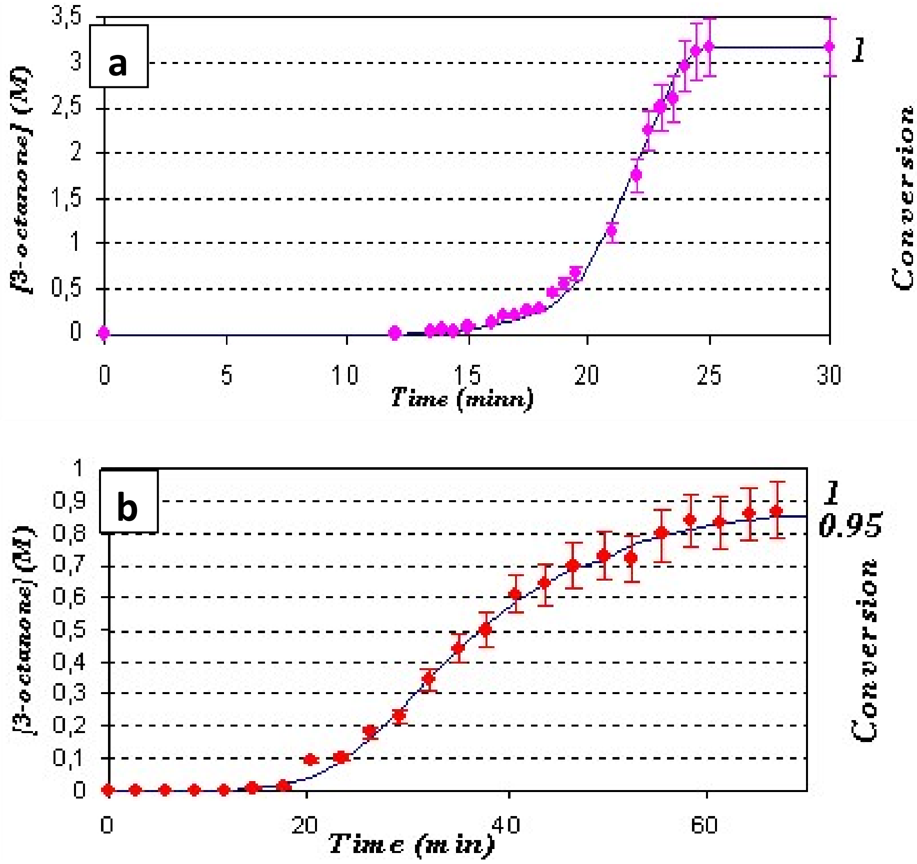

Figure SI 10. Best fit results obtained with ethanol and iso-propanol solvents.

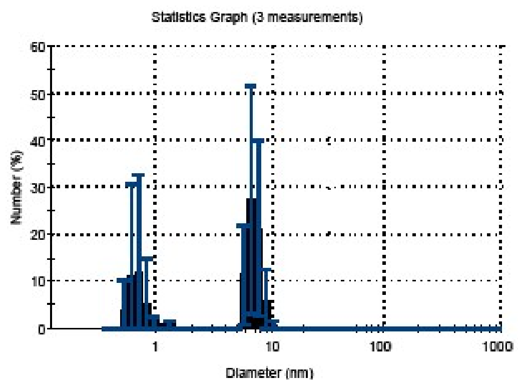

Figure SI 11. DLS measurement results of reaction 1 solution: a - in ethanol as a solvent. Conditions: reaction mixture at the end of induction period, TON= $5.8x10^4$, Conversion = 1.

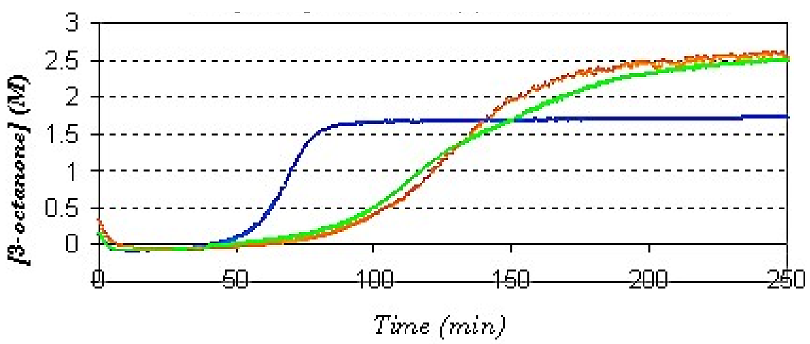

Figure SI 12. The influence of stirring and surfactant addition. Profiles obtained with the following conditions: in iso-propanol, T=80^0C, TON=$1.57x10^5$, $[S]_0$=2.6(M), [cat]=$1.6x10^{-5}$(M): blue line - original conditions, TOF= $1.6x10^3$ (min^{-1}), V_{max}=0.76 (M/min), conversion = 0.65; green line - with stirring, TOF= $0.87x10^3$ (min^{-1}), V_{max}=0.48 (M/min), conversion = 1; orange line - addition of $[aliquat]_0$= 0.068(M) and stirring, TOF= $0.7x10^3$ (min^{-1}), V_{max}=0.03 (M/min), conversion = 1.

a)

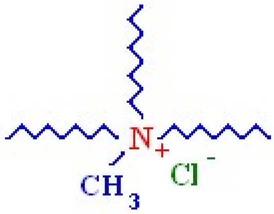

b)

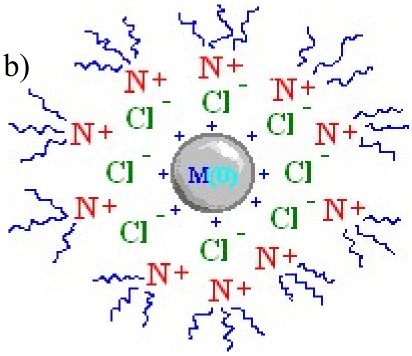

Figure SI 13. Schematics of a) the structure of Aliquat 336; b) stabilization of NPs by Aliquat 336. (*G. Naz, Z. Othaman, M. Shamsuddin, S. K. Ghoshal, Appl Surf Sci* ***2016,*** *363, 74–82)*